International Journal of Mechanical, Industrial and Aerospace Sciences
ISSN: 2517-9950
Vol:10, No:7, 2016

Analysis of Three-Dimensional Longitudinal Rolls Induced by Double Diffusive Poiseuille-Rayleigh-Benard Flows in Rectangular Channels

O. Rahli, N. Mimouni, R. Bennacer, K. Bouhadef

Abstract**—**This numerical study investigates the travelling wave's appearance and the behavior of Poiseuille-Rayleigh-Benard (PRB) flow induced in 3D thermosolutale mixed convection (TSMC) in horizontal rectangular channels. The governing equations are discretized by using a control volume method with third order Quick scheme in approximating the advection terms. Simpler algorithm is used to handle coupling between the momentum and continuity equations. To avoid the excessively high computer time, full approximation storage (FAS) with full multigrid (FMG) method is used to solve the problem. For a broad range of dimensionless controlling parameters, the contribution of this work is to analyzing the flow regimes of the steady longitudinal thermoconvective rolls (noted R//) for both thermal and mass transfer (TSMC). The transition from the opposed volume forces to cooperating ones, considerably affects the birth and the development of the longitudinal rolls. The heat and mass transfers distribution are also examined.

Keywords**—**Heat and mass transfer, mixed convection, Poiseuille-Rayleigh-Benard flow, rectangular duct.

I. Introduction

IN this work, a mixed double diffusive convection in rectangular channels uniformly heated from below and cooled from above has been studied in relation to numerous transport processes where simultaneous heat and mass transfer occur, and which can be encountered in several nature and industrial applications, as cooling of the electronic equipment [1], [2], chemicalvapor deposition (CVD) [3], [4], plastics manufacturing, building sciences [5], [6], moisture transfer and atmospheric flows [7].

In 3D open flows uniformly heated from below so-called PRB configuration, the flow results from superposition of two convective sources: horizontal pressure gradient that causes the main flow within the duct, and a vertical temperature gradient, which is the cause of thermoconvective structures formation. Under the heating effect, when the stability limit is broken, i.e. the Rayleigh Number value is greater than the critical one ($Ra>Ra_c$) several types of thermoconvective rolls may appear, according to the inertial and viscous forces ratio characterized by to the Reynolds number. Indeed, the unstable PRB system is constrained to choose a form of thermoconvective rolls either 3D longitudinal (mono or multi spiral flow) symbolized by ($R_{//}$) or 2D/3D transversal rolls symbolized by ($R_{\perp}$), A combination of transversal and longitudinal rolls can also be observed.

The pioneer experiments about PRB flows are mainly concerned with the meteorological applications [8]. After 1960, the PRB flow studies were mainly based on 2D linear stability analysis and an exhaustive bibliographical review on the PRB flows was exposed by Nicolas [9]. With the combined buoyancy effects, the heat and mass transfer in horizontal square duct was discussed by [10]; a uniform temperature and concentration was assumed at the bottom wall. The authors have found that the buoyancy forces significantly affect the transfers. In addition, under such ducts inclination [11], the results showed that the distributions of local Nusselt (Sherwood) number are characterized by a decay near the inlet in which the forced-convection entrance effect dominates; but the decay is attenuated by the onset of buoyancy-driven secondary flow. At low Reynolds number ($Re \leq 50$) air flow through a bottom heated horizontal plane channel, [12] has shown that the vortex flow pattern changes from longitudinal to transverse rolls when the Reynolds number is lowered or when the Rayleigh number is raised for Re around 10. At a very low Reynolds number, the entire duct is filled with the transverse rolls. Laminar flow of moist air in a 3D rectangular duct with combined heat and mass transfer was investigated [13]. In this numerical and experimental work, the main conclusions founded are that introducing heat gain/loss at the water surface could produce negative heat and mass coefficients and the effects of buoyancy forces were found to be negligible.

In the present work, we focus on the flow structures induced by the additive mass transfer effects, characterized by the coupled thermosolutal buoyancy forces (TSMC), on the heat and mass transfer and its influence on the entrance and fully developed regions.

II. Problem Statement

The geometry of the PRB system considered is a horizontal rectangular duct as schematically shown in Fig. 1. The fluid is assumed incompressible and Newtonian; the laminar flow is governed by 3D incompressible Navier-Stokes model under the Boussinesq assumption.

The duct is heated from the bottom and cooled from the top and constant but different concentrations were imposed on the

O.Rahli is with the Department of Thermal Energy, University of Sciences and Technology Houari Boumediene, Algiers, Algeria (phone: +213 556154436; e-mail: rahliomar@ yahoo.fr).

N. Mimouni and K. Bouhadef are with the Department of Thermal Energy, University of Sciences and Technology Houari Boumediene, Algiers, Algeria (e-mail: n_mimouni@ yahoo.fr, k@ yahoo.fr).

R. Bennacer is with the Department of Civil Engineering, Ecole normale supérieure de Cachan, France (e-mail: rachid.bennacer@ens-cachan.fr).

bottom, C_{heigt}, and on the top wall, C_{low}. At the duct entry the fluid temperature and concentration is at known value. Zero thermal and specie fluxes are imposed on the other longitudinal boundaries.

Mixed convection is controlled by imposing an inlet Poiseuille flow (*i.e.* X= 0). Mass conservation is then maintained by either extracting on the other side the same quantity of matter as in the inlet section, or by using the stress conservation formulation [14].

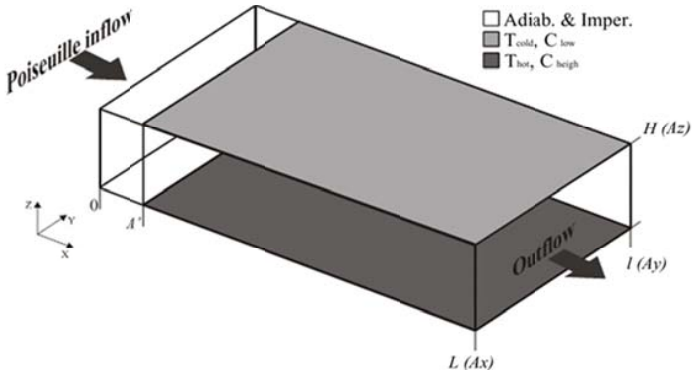

Fig. 1 Physical model

The equations governing the conservation of mass, momentum, energy, and species in non-dimensional variables can be written as:

Continuity equation:

$$\nabla\vec{V} = 0 \tag{1}$$

Momentum equation:

$$\left(\vec{V}\cdot\nabla\right)\vec{V} = -\nabla P + \frac{1}{Re}\nabla^2\vec{V} + \frac{Ra}{Pr\,Re^2}(\theta + NS) \tag{2}$$

Energy equation:

$$\vec{V}\cdot\nabla\theta = \frac{1}{Pr\,Re^2}\nabla^2\theta \tag{3}$$

Diffusion equation:

$$\vec{V}\cdot\nabla S = \frac{1}{Sc\,Re^2}\nabla^2 S \tag{4}$$

The non-dimensional parameters in the above equations are summarized in Table I.

Poiseuille velocity profile $U_{Pois}(y,z)$ for a three-dimensional flow in a channel with finite extensions is the solution of the Poisson's equation (5) with no slip conditions on solid sidewalls.

$$\frac{\partial^2 u_{Pois}}{\partial y^2} + \frac{\partial^2 u_{Pois}}{\partial z^2} = \frac{1}{\mu}\frac{dP}{dx} \tag{5}$$

The analytical solution of this equation is computed in [15].

The boundary conditions in non-dimensional form are as:

– At X = 0:

$$\theta, S = 0;\ U = U_{Pois}(Y,Z);\ V, W = 0 \tag{6}$$

– At X = *Ax*: Outflow non-reflective boundary conditions are imposed.

$$\frac{\partial(\theta,S)}{\partial X} = 0,\ \frac{\partial(V,W)}{\partial X} = 0 \tag{7}$$

$$\text{and}\ \begin{cases} \partial U/\partial X = 0 \text{ mass continuity case} \\ \partial P/\partial n = 2\ \partial^2 U/\partial n^2 \text{ stress continuity case} \end{cases} \tag{8}$$

– At Y = 0 and Y = *Ay*:

$$\partial(\theta, S)/\partial Y = 0 \tag{9}$$

– At Z = 0 and 1:

$$\text{for } X \in [0, A']:\ \frac{\partial(\theta,S)}{\partial Z} = 0 \tag{10}$$

$$\text{for } X \in [A', Ax]:\ (\theta, S) = (1 - Z) \tag{11}$$

– On solid surface

$$\vec{V} = 0 \tag{12}$$

Local Nusselt (*Nu*) and Sherwood (*Sh*) numbers are expressed by:

$$Nu = -\frac{\partial\theta}{\partial Z}\Big|_{Z=0,1} \text{ and } Sh = -\frac{\partial S}{\partial Z}\Big|_{Z=0,1} \tag{13}$$

III. Numerical Method

The governed equations are discretized by using staggered, non-uniform control volumes. In order to minimize the numerical diffusion errors, a third order accurate QUICK scheme with ULTRA-SHARP [16] flux limiter is used in approximating the advection terms. SIMPLE algorithm [17] is used to couple momentum and continuity equations. The momentum equations are solved by applying the strongly

implicit procedure (SIP) [18], which is extended here to handle 3D problems. The discretization of the pressure correction equation results in a set of equations with a symmetric coefficient matrix that is solved by the conjugate gradient (CG) method. In most calculations presented here, under relaxation factor of 0.7 was applied to U, V, W, P, θ and S. To reduce the high computer times inherent in the solution of 3D mixed convection problems, FAS with FMG method [19] is applied to the problem. The equations are solved by a four level fixed V-cycle procedure starting at the coarsest grid and progressing to the finer grid level.

In this work 202 x 202 x 42 irregular grids are used on the finest level. The non-uniform grids have denser clustering near the surface boundaries. To ensure convergence of the numerical algorithm the following criteria is applied to all dependent variables over the solution domain.

$$\frac{\sum\left|\phi_{ijk}^{m}-\phi_{ijk}^{m-1}\right|}{\sum\left|\phi_{ijk}^{m}\right|}\le 10^{-5} \qquad (14)$$

where; ϕ represents a dependent variable U, V, W, P, θ, and S. The indexes i, j, k indicate a grid point; and the index m is the current iteration at the finest grid.

IV. Results And Discussions

Before presenting the results and running our 3D code, we conducted several tests in order to reproduce some previously published results and validate our code. A summary of this part can be found in [20], [21].

The explored cases correspond to some fixed controlling parameter Pr= 0.7, Sc= 0.14 (which corresponds to diffusion of Acetone in air or Benzene in air or Naphthalene in air), Ra = $5x10^3$, A' = 2, Ax = 50, and some others controlling parameters values within the following ranges: Re = 50, 70, $-0.8 \le N \le +0.8$, Ay = 5, 8, 10

Once the PRB system became unstable under the heating effect, it chooses a ($R_{/\!/}$) or ($R_{\perp}$), other intermediary 3D unstable structures are also possible. Several parameters such as *Ra, Re, Pr,* and the boundary layers influence this choice. As illustrated in Fig. 2, the particle describes the helical motion, illustrating the onset of the longitudinal rolls ($R_{/\!/}$). The onset of these thermoconvective structures is due to the combination of the forced convection effect, characterized by the unidirectional Poiseuille inflow, and the secondary convective Rayleigh-Benard (RB) flow obtained under the bottom heating.

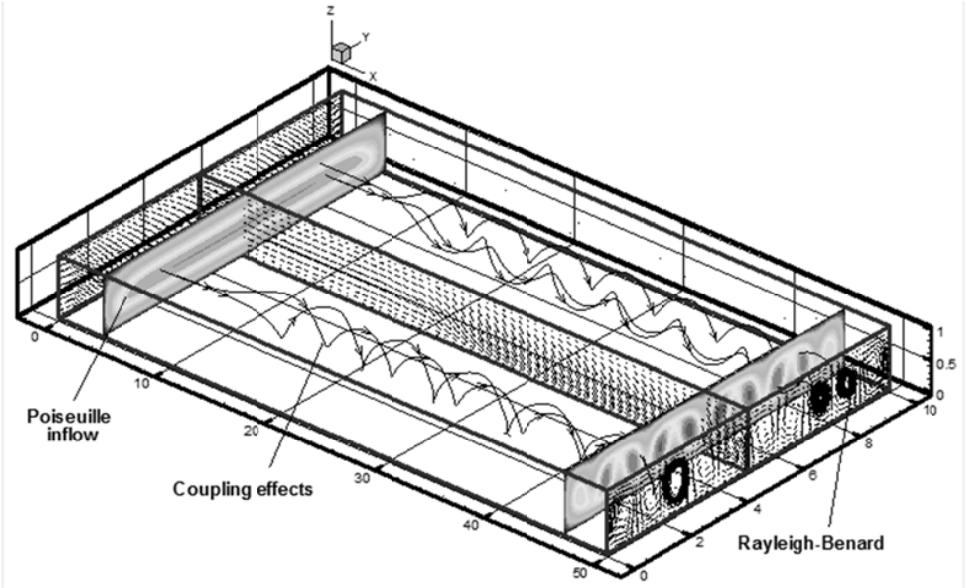

Fig. 2 Streamtraces at the onset of convection

At selected cross-sections shown in Fig. 3, the results clearly indicate that two longitudinal vortex rolls ($R_{/\!/}$) are initiated first from the sidewall region at the upstream (X = 12); on the other channel area, a unidirectional flow remains dominated by the forced convection. As the flow proceeds downstream, more vortex rolls are induced and increase their number in pairs, to reach their fully symmetrically developed state (X = 50) and their maximum number which is equal to the aspect ratio Ay. The rolls dimension is nearly the same as the channel height and the wavelength is around 2. The regular sinusoidal spanwise temperature distributions in accordance with the onset of the steady longitudinal convective rolls, are fully developed from X = 32.

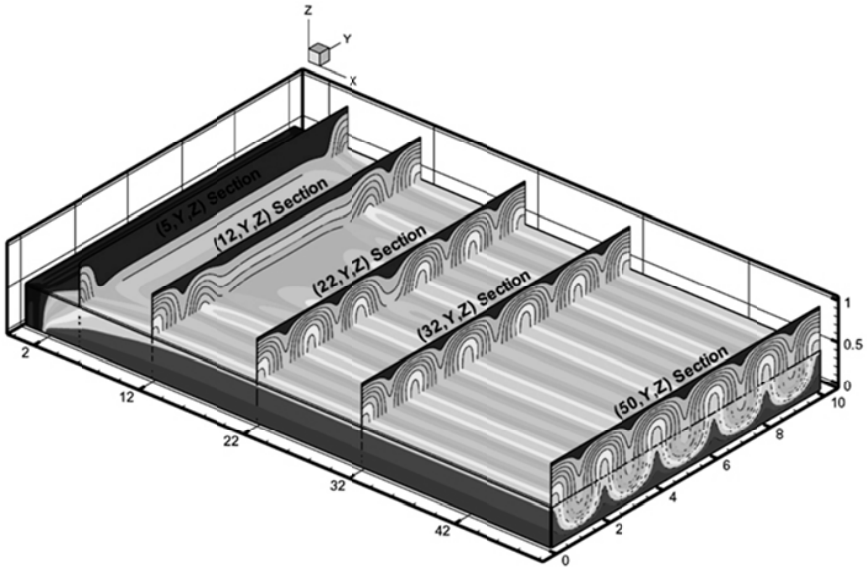

Fig. 3 Steady longitudinal vortex at selected cross-section

The 2D cross sections shown in Fig. 4 clearly indicate that the buoyancy-driven flow distorts the temperature and concentration distributions, and increasing the magnitude of N, more active birth of rolls in space. Indeed, to a fixed axial location X = 12, we see the birth of a single roller for N = -0.5; however, three contra-rotating rolls are already installed for N = 0.8.

The analysis of the oscillatory behavior of the thermal and mass systems further brought forwards the information on variation in the transported heat and mass flux. Fig. 5 represents the longitudinal variation of the local Nusselt and Sherwood numbers for different buoyancy ratio. The curves along the longitudinal axis are seen to provide a monotonic evolution in Nusselt number. Under the particular entrance domain, we can see in this figure a vertical line closer to X = A' and it illustrates the sudden transition between the adiabatic domain and the isothermal boundary conditions, where cold fluid at entrance temperature meets the hot surfaces. The initial decrease in Nu, is attributed to the forced convection entrance effect. The first minimum is reached when the forced convection effect is balanced out by a decrease; owing to the formation of thermal driven secondary flow. After this minimum, an oscillation occurs as the flow goes downstream; and finally, the local Nusselt number gradually reaches an asymptotic situation (established flow), which is waiting for a feature length even weaker than it is closer to the vertical adiabatic walls.

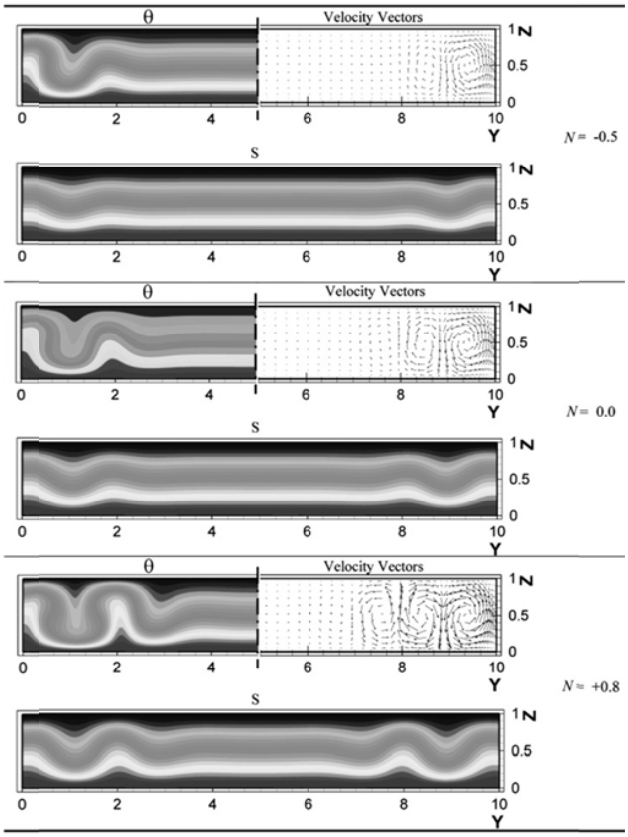

Fig. 4 Velocity vector, temperature and concentration at X = 12 for different value of N

When the buoyancy ratio moves from an opposed state to a cooperating state, buoyancy-driven secondary flow begins to overcome the dominance of the forced convection (minima of Nu) at axial locations (X = X_{SF}) closest to the entrance zone

(see Fig. 5 (a)). This remark also applies to the position where the steady longitudinal rolls R// are fully developed, corresponding to the beginning of stabilization of the Nusselt number represented by the asymptotic values.

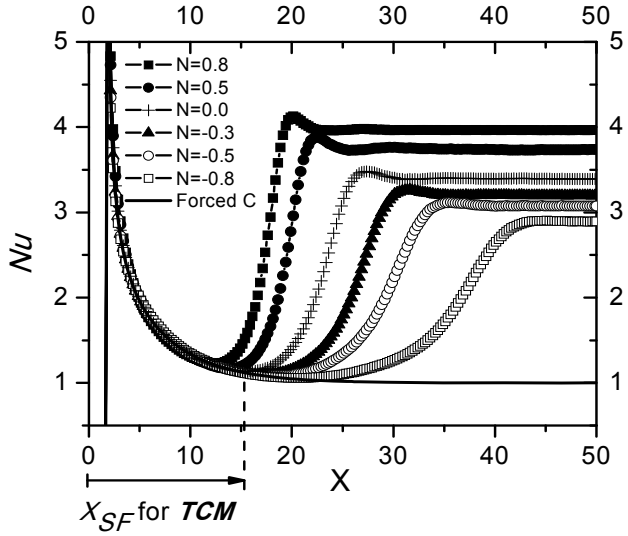

(a)

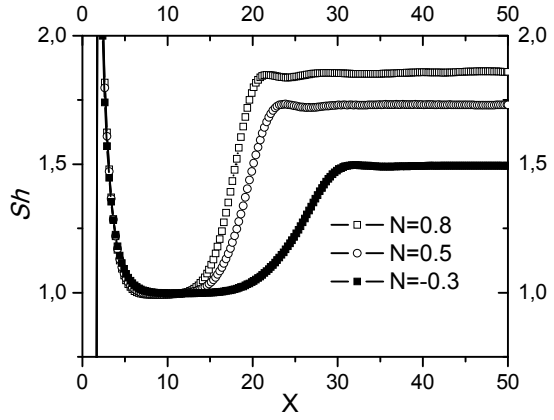

(b)

Fig. 5 Effects of the buoyancy ration on the longitudinal profiles of Nusselt and Sherwood numbers. (a) Nusselt number , (b) Sherwood number

Overall, the evolution of the local Sherwood shows the same variation as the Nusselt number. In addition, we can quote that the installation of convection effects due to Rayleigh-Benard effects will play a role in stabilizing the mass transfer before taking over the effect of forced Poiseuille flow. This is due to the choice of the value of the Lewis number where the Prandlt number is higher than the Schmidt number and the thermal boundary layer develops slower than the concentration boundary layer (Fig. 5 (b)) and as a result, *Nu* is higher than *Sh*; but in general, the exchanges will be promoted with increasing *N*.

The result obtained in Fig. 5 is confirmed in Fig. 6, where it is clearly stated that the onset of mixed convection occurs at distances much closer to the entrance as the buoyancy thermosolutal ratio is high. The increase in Reynolds number promotes the dominance of the forced convective flow. To defeat this flow, we need a greater entrance length. Furthermore, the decrease of parameters *Re* and *Ay*, promotes the reduction of the entrance zone.

Dimensional analysis of the boundary layer thickness in the entrance zone, is controlled by the nature of the fluid and by the interaction between the mixed convection effects, characterized by the Richardson number ($Ri= Ra/Re^2$), and the edge effects related to the elongation *Ay*. However, under the fixed Rayleigh and Prandtl numbers ($Ra = 5x10^3$, $Pr = 0.7$), the analysis carried out from results in Fig. 6, allowed us to predict the position of the onset of the secondary driven flow (*ie:* mixed convection) based on the parameters *N*, *Re* and *Ay*. For the range of parameters chosen, we propose the following correlation:

$$X_{SF} \sim NReAy^{1/2}$$

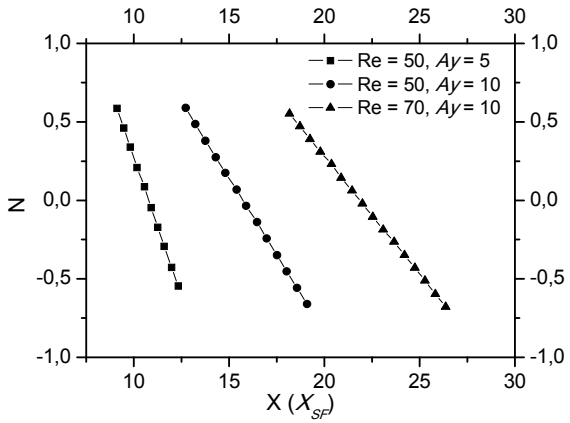

Fig. 6 Effect of buoyancy ratio on the onset of the secondary convective flow

As for the birth of convection, the axial location of the fully developed rolls is linked to the buoyancy effect. Indeed, moving from a state of opposing forces to cooperating forces, the axial location of the fully developed rolls is much closer to the entrance. This reduces the surface area of the triangle entrance region, representing the forced convection dominance zone as shown in Fig. 7. Indeed, the positions shown on the visualizations of temperature fields at selected cross-sections (X,Y,0.5) for different *N* values, are confirmed in the streamtraces represented at (X,5,Z) at the core of the duct. It is clear that the beginning of the streamtrace deviation, initially unidirectional in the entrance zone, corresponds exactly to the position of the fully developed longitudinal rolls. The streamtraces spend from a unidirectional motion (forced convection, Poiseuille flow) to a helical motion generated by the added Rayleigh-Benard (RB) effects to the forced convection effects.

The undertaken simulations have shown that, compared to the total channel length, the length where the rolls are fully developed (L_{PRB}), increases from the buoyancy cooperating effect case (N = +0.8) to the opposite one (N =- 0.5). This is relatively true for the volume of the forced convection dominance zone (represented by a triangle). Note that the order of error for these results is related to the two states of the phenomenon, i.e. fully developed rolls and complete establishment rolls. Indeed, the existence of a transition zone between these two states, where the mixed convection is unstable, arouses our interest to explore more precisely the problem.

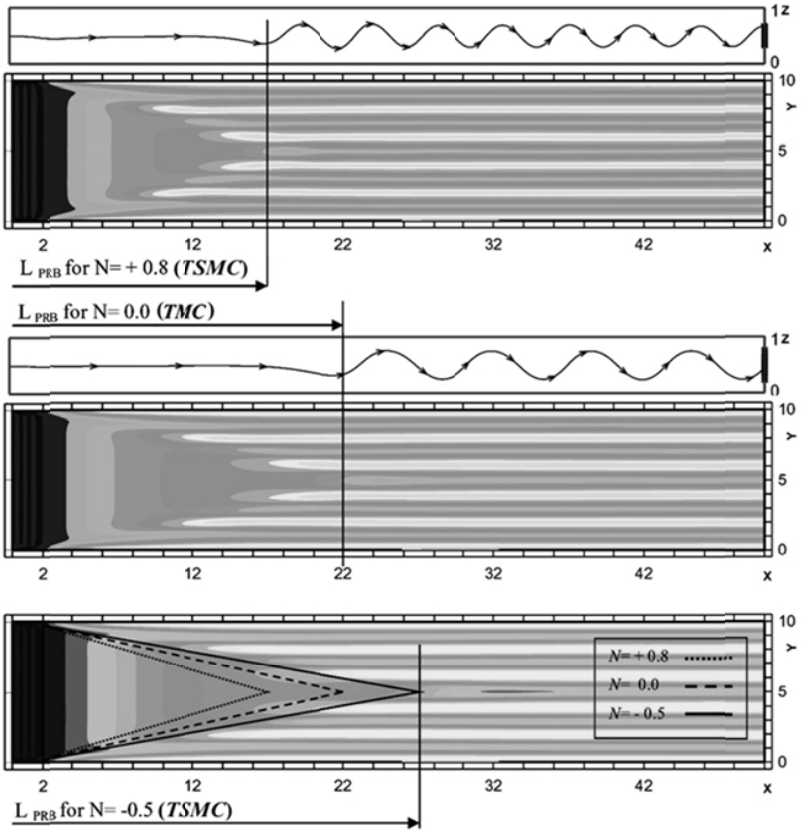

Fig. 7 Effect of buoyancy ratio on the axial location of fully developed rolls (R//) (Temperature fields at plans (X, Y, 0.5) and streamtraces at (X,5, Z) for N = - 0.5, 0 and +0.8)

V. Conclusion

3D laminar double diffusive mixed convection in horizontal rectangular ducts in case of Poiseuille- Rayleigh-Benard flows has been studied numerically. In this work, we focus on the buoyancy forces effect on flow pattern, convective structures and heat and mass transfers, for a selected range of several controlling parameters. The onset of the PRB thermoconvective structures (R//) is due to the combination of the forced convection effect, characterized by the unidirectional Poiseuille inflow, and the secondary convective Rayleigh-Benard flow obtained under the bottom heating.

At fixed Rayleigh number, the onset of buoyancy-driven secondary flow occurs at certain entrance distance depending on the value of buoyancy ratio. This axial location is even lower when the cooperation between the volume forces is greater. The increase in Reynolds number promotes the dominance of the forced convective flow. To defeat this flow, a greater entrance length is needed. Furthermore, the decrease of parameters *Re* and *Ay*, promotes the reduction of the entrance zone. For the range of parameters chosen, we propose that the relation controls the position of the onset of the buoyancy-driven secondary flow as $XSF \sim NReAy^{1/2}$. Quantitatively, this numerical analysis has shown that when the TMC (N=0) case is taken as a reference, our simulations have shown that the length corresponding to the fully developed rolls, will be increased or reduced by of around 22%, respectively, for the cases of opposed TSMC (N=-0.5) and cooperating TSMC (N=+0.8).

TABLE I
NOMENCLATURE

Symbol	Quantity
A'	Entrance aspect ratio
Ax	Longitudinal aspect ratio *L/H*
Ay	Transversal aspect ratio *l/H*
C	Transversal aspect ratio *l/H*
C	Transversal aspect ratio *l/H* concentration
g	gravitational acceleration
H	height of the domain
K_c	wave number
L	length of the domain
l	width of the domain
Nu	Nusselt number
N	buoyancy forces ratio
Pe	Peclet number, *Pe = Re Pr*
Pr	Prandtl number, $Pr = \nu/\alpha$
Ra_T	thermal Rayleigh number, $Ra_T = g\beta_T \Delta T H^3/(\nu\alpha)$
Ra_c	critical Rayleigh number
Re	Reynolds number, $Re = U_{mean}\, H\, /\nu$
T	dimensionless temperature
T_0	reference temperature
ΔT	characteristic temperature difference
ΔC	characteristic concentration difference
S	dimensionless concentration
Sc	Schmidt number
Sh	Sherwood number
U,V,W	dimensionless velocity components
$\vec{V}$	velocity vector
X,Y,Z	dimensionless coordinates system
α	thermal diffusivity $k/(\rho C)$
ρ	fluid density
β	volumetric expansion coefficient
μ	dynamic viscosity
ν	fluid kinematics viscosity
θ	dimensionless temperature
ϕ	dependent variables
	Subscripts
b	bottom
c	cold
eff	effective
f	fluid
h	hot/height
l	low
max	maximum
mean	average value on vertical transversal plan
Pois	Poiseuille
ref	reference value
SF	secondary flow
t	top
⊥	transversal
//	longitudinal

REFERENCES

[1] M. Hasnaoui, E. Bilgen, P. Vasseur, and L. Robillard, Mixed convective heat transfer in a horizontal channel heated periodically from below, Num. Heat Transfer, Part A 20, pp. 297-315, 1991.

[2] S. Q. Zhang, and A.V. Tangborn, Flow regimes in two-dimensional mixed convection with spatially periodic lower wall heating, Phys. Fluids, Vol. 6, pp. 3285-3293, 1994.

[3] N.K. Ingle, and T.J. Mountziaris, The onset of transverse recirculations during flow of gases in horizontal ducts with diferentially heated lower walls, J. Fluid Mech. Vol. 277, pp. 249-269, 1994.

[4] X. Nicolas, A. Benzaoui, and S. Xin, Numerical simulation of thermoconvective flows and more uniform depositions in a cold wall rectangular APCVD reactor. J.of Crystal Growth, Vol. 310, pp. 174-186, 2008.

[5] P. Talukdar, S.O. Olutmayin, O.F. Osanyintola, and C.J. Simonson, An experimental data set for benchmarking 1D, transient heat and moisture transfer models of porous building materials. Part I. Experimental facility and material property data, Int. J. Heat Mass Transfer, Vol. 50, pp. 4527-4539, 2007.

[6] P. Talukdar, O. F. Osanyintola, S. O. Olutmayin, and C. J. Simonson, An experimental data set for benchmarking 1-D, transient heat and moisture transfer models of porous building materials. Part II. Experimental, numerical and analytical data, Int. J. Heat Mass Transfer, Vol. 50, pp. 4915-4926, 2007.

[7] G. Luo, S.P. Vanka, and N. Glumac, Fluid flow and transport processes in a large area atmospheric pressure stagnation flow CVD reactor for deposition of thin films, Int. J. of Heat and Mass Transfer, Vol. 47, pp. 4979-4994, 2004.

[8] D. Brunt, Experimental cloud formation, in: Compendium of Meteorology, American Meteorological Society, Boston, pp. 1255-1262, 1951.

[9] X. Nicolas, Bibliographical review on the PRB flows, Int. J. of Thermal Science, Vol. 41, pp. 961-1016, 2002

[10] J.N. Lin, F.C. Chou, W.M. Yan, P.Y. Tzeng, Combined buoyancy effects of thermal and mass diffusion on laminar forced convection in the thermal entrance region of horizontal square channels, Can. J. Chem. Enging., Vol. 79, pp. 681-689, 1992.

[11] W. M. Yan, Mixed convection heat and mass transfer in inclined rectangular ducts, lnt J. Heat Mass Transfer. Vol. 37, No. 13, pp. 1857-1866, 1994.

[12] M.Y. Chang and T.F. Lin, Experimental study of aspect ratio effects on longitudinal vortex flow in mixed convection of air in a horizontal rectangular duct, Int. J. Heat Mass Transfer, Vol. 41, pp. 719-733, 1998.

[13] W. M. Yan, Combined buoyancy effects of thermal and mass diffusion on laminar forced convection in horizontal rectangular ducts, lnt J. Heat Mass Transfer. Vol. 39, No. 7, pp. 1479-1488, 1996.

[14] T. C. Papanastasiou, N. Malamataris and K. Ellwood, A new outflow boundary conditions. Int. J. Num Meth Fluids, Vol. 14, pp. 587-608, 1992.

[15] A. Benzaoui, X. Nicolas, and S. Xin, Efficient vectorized finite difference method to solve the incompressible Navier-Stokes equations for 3D mixed convection flows in high aspect ratio channels, Numerical Heat TransferB, Vol. 48, pp 277-302, 2005.

[16] B.P. Leonard and S. Mokhtari, Beyond first order upwinding: the ULTRA-SHAP alternative for non-oscillatory steady-state simulation of convection, Int. J. Numerical Methods Eng., Vol. 30, pp. 729-766, 1990.

[17] S.V. Patankar, Numerical Heat Transfer and Fluid Flow, McGraw-Hill, New York, 1980.

[18] H.L. Stone, Iterative solution of implicit approximations of multi-dimensional partial differential equations, SIAM J. Numer. Analysis, Vol.5, pp. 530-558, 1968.

[19] M. Hortmann, M. Peric, and G. Scheuerer, Finite volume multigrid prediction of laminar natural convection: bench-mark solutions, Int. J. Numer. Methods in fluids, Vol. 11, pp. 189-207, 1990.

[20] O. Rahli, R. Bennacer, K. Bouhadef, and D. E. Ameziani, Three-Dimensional Mixed Convection Heat and Mass Transfer in a Rectangular Duct : Case of Longitudinal Rolls, Numerical Heat Transfer, Part A : Applications, 59 : 5, 349-371, 2011.

[21] N. Mimouni, R. Bennacer, S. Chikh and O. Rahli, Limitation of parallel flow in double diffusive convection : Two- and three-dimensional transitions in a horizontal porous domain, Physics of Fluids 26, 074105, 2014.